Results in Chemistry 25 (2026) 103214

Contents lists available at ScienceDirect

Results in Chemistry

journal homepage: www.sciencedirect.com/journal/results-in-chemistry

Solvent-modulated antioxidant activity and molecular binding of a heterocyclic sulfur dipeptide: A spectroscopic and theoretical study

Tatevik Sargsyan [a,b], Silva Jamgaryan [a], Lala Stepanyan [a], Avetis Tsaturyan [a,b], Valentina Mittova [c,d], Zurab R. Tsetskhladze [c,d], Nino Motsonelidze [c,d], Ekaterine Gorgoshidze [c], Niccolò Nova [e,f], Hayarpi Simonyan [b], Karapet Ghazaryan [b], Franco Bisceglie [e], Giovanni N. Roviello [g,*]

[a] Scientific and Production Center "Armbiotechnology" NAS, RA, 14 Gyurjyan Str., Yerevan 0056, Armenia
[b] Institute of Pharmacy, Yerevan State University, 1 Alex Manoogian Str., Yerevan 0025, Armenia
[c] University Geomedi, 4 King Solomon II str., 0114, Tbilisi, Georgia
[d] Scientific-Research Institute of Experimental and Clinical Medicine, University Geomedi, King Solomon II Str. 4, 0114 Tbilisi, Georgia
[e] University of Parma, Department of Chemical Science, Life and Environmental Sustainability, Parco Area delle Scienze 17/A, 43124 Parma, Italy
[f] Aix-Marseille University, CNRS, Central Med, iSm2, 52 Av. Escadrille Normandie Niemen, 13013 Marseille, France
[g] Institute of Biostructures and Bioimaging, Italian National Council for Research (IBB-CNR), Area di Ricerca site and Headquarters, Via Pietro Castellino 111, 80131 Naples, Italy

ARTICLE INFO

Keywords:
Phytotherapy
Caucasus plants
Sulfur dipeptides
Paeonia daurica
Antimicrobial
Antioxidant activity
BSA interaction
Molecular docking

ABSTRACT

A novel sulfur-containing heterocyclic dipeptide (compound 3) was synthesized and preliminarily evaluated for its therapeutic potential in combination with bioactive plant extracts. The antioxidant activity of the dipeptide was assessed using DPPH radical scavenging and phosphomolybdate assays. In the DPPH assay, compound 3 exhibited dose-dependent activity, with IC_{50} values of 2.39 ± 0.24 mg/mL in methanol and 2.84 ± 0.29 mg/mL in DMSO, indicating greater efficacy in methanol. Conversely, the phosphomolybdate assay revealed higher total antioxidant capacity in DMSO, suggesting solvent-dependent behavior. Antibacterial activity was tested against *Escherichia coli* ATCC 25922 using the Kirby–Bauer diffusion method. While compound 3 alone showed no inhibitory effect at concentrations up to 50 mg/disk, its combination with methanolic extracts of *Paeonia daurica* subsp. *mlokosewitschii* (leaves and roots) resulted in a dose-dependent modulation of the plant extracts' antibacterial activity, indicating an interaction that may influence phytotherapeutic efficacy. Independently, the plant extracts demonstrated measurable antibacterial activity, with inhibition zones of 13.61 ± 0.17 mm (leaves) and 13.75 ± 0.05 mm (roots) at 200 μg/disk. Circular dichroism (CD) spectroscopy using bovine serum albumin (BSA) revealed specific peptide–protein binding interactions, supporting the biological relevance of the dipeptide. These findings were further supported by Density Functional Theory (DFT) calculations, molecular docking, and CD spectral deconvolution, providing insight into the compound's structural and interaction properties. Overall, the study highlights the potential of compound 3 as a modulator of plant-derived bioactivities and its relevance in the development of synergistic therapeutic strategies.

Abbreviations: AMP, Antimicrobial Peptide; ATR, Attenuated Total Reflection; BFEN-O, Bond Formation Enthalpy of the Oxidized Species; BFE, Bond Formation Energy; BSA, Bovine Serum Albumin; CD, Circular Dichroism; CFU, Colony-Forming Unit; $CHCl_3$, Chloroform; DCC, Dicyclohexylcarbodiimide; DCU, Dicyclohexylurea; DFT, Density Functional Theory; DMSO, Dimethyl Sulfoxide; DPPH, 2,2-Diphenyl-1-picrylhydrazyl; ESI-MS, Electrospray Ionization Mass Spectrometry; EtOAc, Ethyl Acetate; Fmoc, 9-Fluorenylmethoxycarbonyl; FMO / FMOs, Frontier Molecular Orbital(s); HOSu, N-Hydroxysuccinimide; HOMO, Highest Occupied Molecular Orbital; HPLC, High-Performance Liquid Chromatography; IC_{50}, Half Maximal Inhibitory Concentration; IP, Ionization Potential; IR, Infrared; K2D2, Computational Tool for CD Spectrum Deconvolution; KBr, Potassium Bromide; LB, Luria-Bertani (broth/agar); LCMS, Liquid Chromatography–Mass Spectrometry; LUMO, Lowest Unoccupied Molecular Orbital; MeOH, Methanol; MEP, Molecular Electrostatic Potential; m/z, Mass-to-Charge Ratio; MMFF, Merck Molecular Force Field; $NaHCO_3$, Sodium Bicarbonate; NaOH, Sodium Hydroxide; Na_2CO_3, Sodium Carbonate; ncAA, Non-Canonical Amino Acid; NHS, N-Hydroxysuccinimide 1; NMR, Nuclear Magnetic Resonance; PBS, Phosphate-Buffered Saline; PDB, Protein Data Bank; RMSD, Root Mean Square Deviation; ROS, Reactive Oxygen Species; RSA%, Radical Scavenging Activity Percentage; S.D., Standard Deviation; SET, Single Electron Transfer; SMILES, Simplified Molecular Input Line Entry System; TAC, Total Antioxidant Capacity; TD-SCF, Time-Dependent Self-Consistent Field; TLC, Thin-Layer Chromatography; TMS, Tetramethylsilane; UV / UV–vis, Ultraviolet / Ultraviolet–Visible Spectroscopy; VMD, Visual Molecular Dynamics.

* Corresponding author.
E-mail address: giovanni.roviello@cnr.it (G.N. Roviello).

https://doi.org/10.1016/j.rechem.2026.103214
Received 20 December 2025; Accepted 5 March 2026
Available online 6 March 2026
2211-7156/© 2026 The Authors. Published by Elsevier B.V. This is an open access article under the CC BY license (http://creativecommons.org/licenses/by/4.0/).

1. Introduction

In the evolving landscape of therapeutic discovery, the integration of peptides with natural products has become a central focus of phytotherapy research. This multidisciplinary field seeks to harness the therapeutic potential of plant-derived molecules while enhancing efficacy, stability, and target specificity through strategic combination with synthetic agents. Particularly in the context of rising antimicrobial resistance and the increasing prevalence of oxidative stress-related disorders, there is a pressing need for innovative, dual-function systems that unify the bioactivity of natural extracts with the precision of synthetic peptide chemistry. *Paeonia daurica* subsp. *mlokosewitschii* (Lomakin) D. Y. Hong is a representative of the family *Paeoniaceae* [1,2], a perennial herbaceous species characterized by biternate foliage in shades of grey or grey-green, broad yellow flowers, and a lignified, branched system of rhizomes and roots [3]. The species exhibits endemism to the Caucasus region, being distributed from the middle montane zone to the upper zone, in the forest, on stony slopes of the North Caucasus and Transcaucasus (Plants of Worlds Online; retrieved from https://powo.science.kew.org/ (accessed on 05.05.2025)). In Georgia, it is distributed exclusively in two main areas: Kiziki (Shiraki) and Kakheti (Lagodekhi) [4]. Notably, *Paeonia* genus extracts are commonly employed in traditional medicine across numerous regions, especially in Asia, which suggests their recognized ethnopharmacological significance [5]. However, the therapeutic properties and phytochemical composition of *Paeonia daurica* subsp. *mlokosewitschii* have not been investigated. Nevertheless, it is known that leaves and roots of several *Paeonia* species are endowed with antibacterial, antioxidant, antitumor, anti-inflammatory, analgesic, neuroprotective and hypotensive properties [6–11]. A comprehensive analysis of various *Paeonia* species has identified a diverse array of compounds, including 15 stilbenes, 49 triterpenoids, and steroids, 53 tannins, 59 flavonoids, 153 monoterpenoid glucosides, 61 phenolic compounds, and an additional 61 substances, as summarized in reference [12].

Tackling socially impactful diseases drives the development of innovative therapeutic approaches involving molecular platforms that integrate both natural and synthetic compounds, including peptides, oligonucleotides, and hybrid architectures like nucleobase-containing peptides [13–21]. Recent studies have demonstrated that hybrid formulations combining plant extracts with synthetic drugs can result in synergistic or modulatory effects, offering novel pathways for therapeutic intervention [22]. Antimicrobial plant extracts exert a significant influence on the human microbiome, with various tested extracts modifying gut microbial basal conditions following in vitro fermentation, often in an inhibitory manner [23]. This pronounced suppressive effect emphasizes the necessity of developing new additives that can attenuate excessively strong antimicrobial action. By fine-tuning these formulations, researchers can help maintain microbial balance while still obtaining the beneficial properties of plant-derived compounds for health applications. Within this framework, sulfur-containing aromatic peptides, known for their stability, lipophilicity, and tunable interactions with biological targets, are emerging as valuable tools to modulate the pharmacological profile of plant extracts. Although not all peptides exhibit direct antimicrobial activity, many bioactive peptides represent some of the most promising antimicrobial candidates due to their biocompatibility, structural diversity, and ability to selectively target microbial and cellular components. These peptides exhibit diverse therapeutic capabilities, including anticancer, antioxidant, and enzyme-inhibitory activities [24–32].

The bioactive potential of peptides is primarily influenced by the amino acids they contain, each contributing specific physicochemical properties that collectively shape the peptide's biological activity. Studies have shown that leucine, a hydrophobic, branched-chain essential amino acid, plays a crucial role in peptide design by enhancing structural stability and promoting interactions with biological membranes. Although leucine itself is not intrinsically antimicrobial, leucine-rich peptide sequences have been shown to influence peptide conformation and facilitate membrane disruption, thereby contributing to overall bioactivity. Hydrophobicity plays a key role in determining how water-soluble peptides integrate into the membrane lipid bilayer, a process crucial for membrane permeabilization [33–38].

Incorporating non-proteinogenic amino acids is a strategic approach to modulating the pharmacological profile of peptides [39–42]. Among these, 1,2,4-triazole-based amino acid derivatives have garnered considerable attention due to their chemical stability and broad-spectrum bioactivities, including enzyme-inhibitory effects. These heterocyclic motifs frequently disrupt critical microbial pathways, such as cytochrome P450-dependent ergosterol biosynthesis, while concurrently enhancing peptide stability and membrane permeability. In recent years, peptides bearing sulfur-containing heterocyclic moieties – such as thiazoles and thiophenes – have attracted growing interest for their distinctive physicochemical characteristics, including increased lipophilicity, conformational rigidity, and improved biomolecular interactions. These structural features enhance binding affinity to key biological targets, particularly nucleic acids and serum proteins, thereby contributing to the therapeutic potential of peptide-based scaffolds [43–50]. Such properties make these peptides excellent candidates for modulating the antimicrobial activity of bioactive plant extracts, where they can fine-tune extract efficacy and improve therapeutic profiles by influencing both the microbial membrane interactions and the stability of the active compounds. Interestingly, hybrid peptide systems that integrate natural amino acids (e.g., glycine, alanine, leucine) with bioactive heterocycles represent a rational strategy for the development of next-generation therapeutics that exhibit both antioxidant activity and membrane-disrupting capabilities, a combination whose relevance is further validated by peptides' rapid mode of action in the treatment of infections associated with oxidative stress [51–54].

In the present study, we report the synthesis of a novel dipeptide containing 1,2,4-triazole and sulfur-based heterocycles, incorporating a Fmoc (9-fluorenylmethoxycarbonyl)-protected amino acid residue. Remarkably, Fmoc groups, commonly used in peptide synthesis, not only facilitate purification and improve peptide solubility but also enhance bioavailability through increased lipophilicity [55,56]. The combination of sulfur-based heterocycles and Fmoc protection presents a synergistic strategy for designing peptides with improved pharmacokinetics and target-binding capabilities. The new dipeptide 3 with plant extract-modulatory properties was synthesized and its biological properties were evaluated through preliminary studies on the peptide modulatory effects on *Paeonia daurica* extracts, antioxidant assays and interaction studies with bovine serum albumin (BSA).

2. Experimental section

2.1. Synthesis and purification of materials

In this study, we used the following chemicals: DCC, dimethylsulfoxide (DMSO), N-hydroxysuccinimide, DPPH (2,2-diphenyl-1-picrylhydrazyl), C_6H_{14}, $C_4H_8O_2$, $CH_3COOC_2H_5$, Na_2CO_3, $NaHCO_3$, NaOH, (*S*)-2-((((9H-fluoren-9-yl)methoxy)carbonyl)amino)-4-methylpentanoic acid (1), ammonium molybdate, CH_2Cl_2, methanol obtained from Sigma-Aldrich (St. Louis, MA, USA). The LB agar plates and LB broth for *E. coli* were purchased from LLC Elavia Biopreparations, Tbilisi, Georgia. The compound (*S*)-2-amino-3-(4-phenyl-3-propyl-5-thioxo-4,5-dihydro-1H-1,2,4-triazol-1-yl)propanoic acid (2) was synthesized at the Armbiotechnology Scientific and Production Center, National Academy of Sciences (Armenia) [57]. All reagents were obtained from commercial sources and employed in the study without undergoing additional purification. Solvents were freshly distilled prior to use. Thin-layer chromatography (TLC) analyses were conducted using Merck aluminum-backed plates coated with 0.2 mm Kieselgel 60 F254 (Darmstadt, Germany). Proton (^{1}H) and carbon-13 (^{13}C) NMR spectra were acquired

using a Varian Mercury 300 MHz spectrometer, with tetramethylsilane (TMS) serving as the internal reference (Palo Alto, CA, USA). Melting points were assessed via an electrothermal device from Bibby Scientific (Stone, UK). LCMS measurements were performed using a Shimadzu LCMS 2020 system coupled with a Prominence-I LC-2030C 3D unit. Infrared spectral analysis was carried out employing an ATR (Attenuated Total Reflection) module, enabling direct evaluation of powdered samples with a Shimadzu IRTracer-100 spectrometer (Kyoto, Japan), utilizing a KBr prism (4000–350 cm^{-1}) in single reflection mode at a resolution 4 cm^{-1}.

Preparation of the *N*-Oxysuccinimide ester: a solution containing 0.4 g (1.14 mmol) of amino acid 1 and 0.15 g (1.3 mmol) of N-hydroxysuccinimide (NHS) was prepared in 2.0 mL of dioxane and 2.0 mL of methylene chloride. To this mixture, 0.25 g (1.21 mmol) of dicyclohexylcarbodiimide (DCC), pre-dissolved in 2 mL of dioxane, was added at 0 °C. The reaction was maintained at this temperature for 1 h, followed by an additional hour at room temperature. Progress was monitored via thin-layer chromatography (TLC) using a solvent system of chloroform/ethyl acetate/methanol (2:4:1). Upon completion, the precipitated dicyclohexylurea (DCU) was removed by filtration. The resulting filtrate, containing the succinimide ester intermediate, was concentrated under reduced pressure to yield an oily residue. This intermediate was obtained in 0.38 g (75% yield) and used directly in the subsequent peptide coupling step.

Synthesis of dipeptide 3: to a solution of 0.34 g (1.1 mmol) of amino acid 2 in 1.6 mL of 0.5 M NaOH, 0.034 g (0.4 mmol) of sodium bicarbonate was added. Subsequently, 0.36 g (0.8 mmol) of the N-hydroxysuccinimide ester of (*S*)-2-((((9H-fluoren-9-yl)methoxy)carbonyl) amino)-4-methylpentanoic acid, dissolved in 2 mL of dioxane, was introduced. The reaction mixture was stirred at room temperature for 3 h. After completion, the mixture was transferred to a separatory funnel, and 6 mL of ethyl acetate, 3 mL of 10% citric acid solution, and 0.2 g of sodium chloride were added. Vigorous stirring facilitated phase separation. The organic layer was collected, dried over magnesium sulfate, and the solvent was removed under vacuum at 50 °C. The residue was crystallized from a 1:3 mixture of ethyl acetate and petroleum ether, yielding dipeptide 3 as a white crystalline solid (67% yield; mp: 122–125 °C).Characterization of 3 (Fig. S1–S5) - ESI MS (*m/z*): 641.79 (expected); 642.10 (found).

ATR-IR, ν, cm^{-1}: 3649.32 (N—H), 3568.31 (N—H), 2927.94, 2870.08 (C—H, aliphatic), 1716.65 (C═O, acid/ester), 1670.35 (C═O, carbamate), 1496.76 (C═N, carbamate), 1446.61 (C═C, aromatic), 1408.04 (C—N, aromatic), 1330.88 (C=S), 1161.15 (C—O, acid), 1107.14 (C—O, ether), 1072.42, 1041.56 (C—N, heterocyclic), 1010.70 (C—N, heterocyclic), 759.95, 736.81 (C—H, aromatic bending).

^{1}H NMR (300 MHz, DMSO/CCl4 1/3, δ, ppm, Hz): 0,81 t (3H, J = 7.3, CH_3), 0.90 d (3H, J = 6.8, CH_3), 0.92 d (3H, J = 6.8, CH_3), 1.45–1.59 m (4H, 2·CH_2), 1.68 m (1H, 2·CH_3), 2.28–2.42 m (2H, $CH_2C_2H_5$), 4.00–4.06 m (1H), 4.09–4.19 m (2H), 4.31–4.39 m (2H), 4.68 br d (1H, J = 12.6), 4.83 m (1H), 7.20–7.28 m (3H), 7.31–7.37 m (4H), 7.45–7.52 m (3H), 7.59–7.69 m (3H), 7.71–7.75 m (2H). ^{13}C NMR (75 MHz, DMSO/CCl4 1/3, δ, ppm): 13.1, 18.8, 21.1, 23.1, 24.0, 26.9, 29.0, 40.9, 46.6, 50.6, 53.2, 65.7, 119.29, 119.32, 125.0, 125.1, 126.5, 127.0, 128.0, 128.79, 128.82, 134.3, 140.5, 143.5, 143.6, 149.7, 155.5, 167.4, 171.2.

2.2. CD experiments

CD measurements were carried out using a Chirascan™ V100 spectropolarimeter (Applied Photophysics, Leatherhead, Surrey, UK) equipped with a Peltier Quantum temperature control unit. Experiments were conducted at 15 °C in a 10 mM phosphate-buffered saline (PBS) solution at pH 7.4. Compound 3 was prepared as a 9 mM stock solution in acetonitrile. For each measurement, 1.8×10^{-2} nmol of BSA (Merck, Darmstadt, Germany) and 9 nmol of compound 3 were combined. The final sample volume was 0.15 mL, and spectra were recorded using a quartz cuvette with a 0.5 mm path length (Applied Photophysics, Leatherhead, Surrey, UK). Each CD spectrum represented the average of three consecutive scans. To isolate the spectral contribution of the BSA–compound 3 complex, the CD spectrum of compound 3 alone was subtracted from the composite signal.

2.2.1. CD deconvolution

The alpha-helix and beta-sheet contents of the serum albumin before and after the addition of the analyzed compound were estimated using the K2D2 program (freely available at the link https://cbdm-01.zdv.uni-mainz.de/~andrade/k2d2/ accessed on 03 October 2025 [58]), which predicts secondary structure starting from circular dichroism data. These data in the wavelength range 190 to 240 nm were selected for our analysis, with a total of 51 data points that were used as input for each spectrum.

For BSA alone, the CD (mdeg) values from 190 to 240 nm were: 13.1288, 13.4629, 13.5829, 13.3857, 12.79, 11.7945, 10.4201, 8.70985, 6.72956, 4.52588, 2.2591, 0.082393, −1.89345, −3.67701, −5.19778, −6.39, −7.33068, −7.9885, −8.38384, −8.52532, −8.48471, −8.35751, −8.15085, −7.99124, −7.8414, −7.75435, −7.72313, −7.71971, −7.73458, −7.72911, −7.74177, −7.75027, −7.70481, −7.63183, −7.50136, −7.28702, −7.01011, −6.62888, −6.1975, −5.73109, −5.25258, −4.73771, −4.2365, −3.74054, −3.2951, −2.84898, −2.45421, −2.0776, −1.76358, −1.51291, −1.2978.

For BSA in complex with compound 3, the CD mdeg values from 190 to 240 nm were: 13.6587, 13.9424, 13.9272, 13.7173, 13.2737, 12.3979, 11.2392, 9.65727, 7.7536, 5.64038, 3.46379, 1.28454, −0.637425, −2.32598, −3.78598, −4.97289, −5.83548, −6.49397, −6.87931, −7.0685, −7.11813, −7.03134, −6.79583, −6.66326, −6.59235, −6.53253, −6.49102, −6.4893, −6.49729, −6.56534, −6.63871, −6.60897, −6.5675, −6.4955, −6.35212, −6.1132, −5.79559, −5.41274, −5.0218, −4.64916, −4.23807, −3.75557, −3.29432, −2.86315, −2.47852, −2.03144, −1.60917, −1.28886, −1.02526, −0.814446, −0.629929.

2.3. Antioxidant activity assessment

2.3.1. DPPH radical scavenging assay

Stock solutions of dipeptide 3 (10 mg/mL) were prepared using either 99.9% methanol or 99.9% DMSO as solvents. The antioxidant activity of dipeptide 3 was evaluated following the procedure outlined in reference [59]. For each test, 200 μL of dipeptide 3 at varying concentrations was combined with 2.8 mL of a 0.1 M DPPH solution in methanol, resulting in final concentrations ranging from 50 to 500 μg/mL. These concentration values were selected based on prior optimization experiments. The mixtures were incubated in the dark at room temperature for 30 min. Absorbance readings were taken at 517 nm using a DU-8800 RS spectrophotometer (Drawell, China). A methanolic DPPH solution served as the blank, with an absorbance value of 0.98 ± 0.02. Radical scavenging efficiency was calculated as the percentage reduction in DPPH absorbance. The IC_{50} values, representing the concentration of dipeptide 3 required to inhibit 50% of the DPPH radicals, were determined by plotting inhibition percentages against sample concentrations and applying linear regression analysis.

$$Y = a \bullet X + b$$

$$IC_{50} = \frac{(50 - b)}{a}$$

2.3.2. Assessment of the total antioxidant capacity (Phosphomolybdate Assay)

The total antioxidant capacity (TAC) of dipeptide 3 was evaluated using the phosphomolybdate assay, with ascorbic acid serving as the reference standard [60]. Varying concentrations of dipeptide 3 (200 μL)

were combined with 2.8 mL of reagent solution composed of 0.6 M sulfuric acid, 28 mM sodium phosphate, and 4 mM ammonium molybdate, yielding final concentrations ranging from 30 to 450 μg/mL. The reaction mixtures were sealed and heated in a water bath at 95 °C for 90 min. Following cooling to room temperature, absorbance was recorded at 765 nm using a blank for baseline correction. Results were expressed in terms of ascorbic acid equivalents (AAE) per μg/mL of dipeptide 3. The blank consisted of 2.8 mL of reagent solution and 200 μL of solvent, subjected to identical incubation conditions.

2.4. Assessment of the antimicrobial activity

2.4.1. Extraction of plant samples

Paeonia daurica subsp. *mlokosewitschii* (Lomakin) D. Y. Hong plant specimens were harvested in July 2024 from the National Botanical Garden of Georgia, located in Tbilisi (GPS coordinates: N 41.68574°, E 44.80217°). A portion of leaves and roots (5 g each) was subjected to freeze-drying using a DW-10 N freeze dryer (Drawell, China) within a 500 mL vacuum flask at a pressure of 10 Pa and a condenser temperature of −55 °C, continuing until a stable dry weight was achieved. The dried plant material was then homogenized in a 1:5 ratio with 80% methanol, selected based on its superior extraction efficiency [61,62]. The mixture was stirred continuously for 24 h at room temperature using an orbital shaker operating at 270 rpm. Following extraction, the crude solutions were clarified by centrifugation at 5000*g* for 15 min using a TD6 Benchtop Centrifuge (Drawell, China). The resulting methanolic leaf and root extracts were concentrated via rotary evaporation at 50 °C using a DW-ORE2000 Rotary Evaporator (Drawell, China), and the final residues were reconstituted in 80% DMSO.

2.4.2. Determination of antibacterial activity

The antibacterial activity evaluation was performed with the Kirby-Bauer diffusion method [62]. The *Escherichia coli* ATCC 25922 strain, cultured in LB broth for 16–18 h at 37 °C to reach a density of approximately 10^9–10^{10} CFU/mL, was employed for antibacterial testing. Sterile 6 mm blank discs were placed on LB agar plates inoculated with 300 μL of the bacterial suspension. Each disc was treated with 10 μL of dipeptide 3 dissolved in DMSO, at concentrations ranging from 5 to 50 μg/disk. For experiments involving plant extracts, leaf or root extracts of *Paeonia daurica* subsp. *mlokosewitschii* (200 μg/disk) were applied individually to the discs. To evaluate the modulatory effect of dipeptide 3 on the antibacterial activity of these extracts, varying amounts of dipeptide 3 (12–25 μg/disk) were combined with either leaf or root extracts (200 μg/disk), maintaining a total application volume of 10 μL per disc. All plates were incubated at 37 °C for 24 h. Antimicrobial efficacy was assessed in triplicate by measuring the diameter of the inhibition zones (mm). Amoxicillin (30 μg/disk) served as the positive control, while 80% DMSO was used as the negative control.

2.5. Statistical analysis

All experiments were conducted in triplicate, and the resulting data are presented as mean values accompanied by their respective standard deviations. Statistical comparisons were carried out using a variance-based *t*-test implemented in Microsoft Excel 365. A *p*-value below 0.05 was interpreted as indicative of a statistically significant difference.

2.6. Molecular docking

Blind docking simulations were conducted using the HDOCK platform, which applies the ITScore-PP algorithm, an iterative, knowledge-based scoring method, to rank the top ten predicted binding poses. The software generates a dimensionless energy value, referred to as the HDOCK score, where lower scores correlate with stronger binding affinities. These computational predictions have shown good agreement with experimental data. For downstream analysis, the highest-ranked pose (Top-1) was selected based on its energy score. The peptide structure used for docking was generated through a multi-step process. First, the SMILES representation was derived from the IUPAC name using MolView. This string was then submitted to the ProNovo online tool (https://novoprolabs.com/tools/smiles2pdb; accessed April 9, 2025), which converted it into a 3D PDB format. The resulting file was refined in Discovery Studio Biovia (BIOVIA, Dassault Systèmes, San Diego, CA, USA), where hydrogen atoms were added and energy minimization was performed using the MMFF force field. The finalized structure was uploaded to HDOCK for blind docking against BSA, using PDB ID 4F5S as the target. Default parameters were applied throughout the docking procedure. Additional information about the HDOCK platform is available at http://hdock.phys.hust.edu.cn/ (accessed on 11 Jun 2025).

SMILES (compound 3).

C1C2=C(C3C(C2COC(N([H])[C@@](CC(*C*)C)C(N([H])[C@@](CN2C(=S)N(C4C=CC=CC=4)C(CCC)=N2)C(O[H])=O)=O)=O)=CC=CC=3)C=CC=1

2.7. Computational evaluation (DFT)

Over recent decades, Density Functional Theory (DFT) calculations have proven to be a powerful tool for understanding the antioxidant properties of several compounds [63–68]. Computational modeling was carried out using Gaussian 16 [69], with GaussView 6 serving as the graphical interface. Geometry optimizations for the peptide structure were performed in both singlet and triplet electronic states using density functional theory (DFT) at the ωB97XD/6-31+G(d,p) level. The inclusion of polarization and diffuse functions was intended to improve the reliability of calculations regarding polar bonds and to adequately represent sulfur-containing groups [70]. Additionally, geometry optimizations were carried out under methanol and DMSO solvation conditions using the polarizable continuum solvation model (CPCM) [71], followed by frequency calculations in each solvent to obtain thermodynamic properties. Structural superimpositions and RMSD (Root Mean Square Deviation) values were calculated using VMD software. Log(P) value was calculated through ChemDraw 22.2.0 suite.

The spatial distribution of surface charge was illustrated using Molecular Electrostatic Potential (MEP) maps [67,72], which depict the electrostatic potential (ESP) across the molecular surface, reflecting the cumulative influence of atomic nuclei and surrounding electron density. The contribution to the ESP depends on the distance from the evaluated point: nuclei have a positive influence, while electrons have a negative one, as illustrated by the equation provided in the Supporting Information for a generic vector position.

Frontier Molecular Orbitals (FMOs) were analyzed by evaluating the HOMO/LUMO energy gaps under each condition to compare outcomes with experimental results. Having regard for the radical scavenging mechanism of DPPH toward the peptide through single-electron transfer (SET), this pathway was investigated both in the gas phase and under solvation [64–67] [73]. Moreover, the formation enthalpies (BFE) of the oxidized thioxo-triazole ring derivative were computed [74], given that phosphomolybdate could oxidize the peptide through this route. The SET mechanism was evaluated using the Ionization Potential (IP), while the TAC assay was interpreted in terms of Bond Formation Energy (BFE):

$$ArOH \rightarrow ArOH^{+} + e^{-}$$

$$IP = H(ArOH^{+}) - H(ArOH)$$

$$ArN + O \rightarrow [ArN^{+} - O^{-}]$$

$$BFE_{N-O} = H([ArN^{+} - O^{-}]) - H(ArN) - H(O)$$

where H stands for total enthalpy (Hartree).

A time-dependent self-consistent field (TD-SCF) calculation was

performed using the ωB97XD density functional over the 6-31+G(d,p) basis set, with methanol modeled as the solvent. This computational approach was employed to simulate electronic transitions and compare them with the experimental UV–Vis absorption spectrum (Fig. S6) [67,75].

3. Results and discussion

3.1. Peptide Synthesis and BSA binding studies

Dipeptide 3, incorporating the non-proteinogenic amino acid 1, was synthesized according to the protocol illustrated in Scheme 1. The initial step involved converting the protected amino acid 1 into its succinimide ester derivative. This transformation was achieved by activating the carboxyl group of the Fmoc-amino acid using N-hydroxysuccinimide (NHS) in the presence of dicyclohexylcarbodiimide (DCC) as the coupling agent. The reaction was carried out in a solvent mixture of dioxane and methylene chloride, yielding a stable NHS ester intermediate.

Subsequently, amino acid 2 was coupled with the NHS-activated Fmoc-amino acid 1 to form the dipeptide. Various reaction conditions were explored, particularly focusing on the molar ratio of sodium hydroxide (NaOH) to sodium carbonate (Na_2CO_3). The most favorable outcome was achieved with a NaOH:Na_2CO_3 ratio of 1:0.5, which significantly reduced the formation of side products. In contrast, reactions performed using NaOH alone resulted in a higher incidence of undesired by-products. Under optimized conditions, dipeptide 3 was successfully synthesized, as depicted in Scheme 1.

As anticipated, the synthesis of dipeptide 3 was achieved starting from Fmoc-protected amino acid 1, employing HOSu and DCC to activate the carboxyl groups. This strategy is favored due to the stability of the reactive intermediates, which facilitates efficient coupling with a range of amino acids. Reaction conditions were optimized by varying the molar proportions of NaOH and Na_2CO_3, leading to the identification of an optimal ratio of 1:0.5 (NaOH:Na_2CO_3), which effectively reduced the formation of undesired side products. This optimized protocol not only enabled the successful preparation of dipeptide 3 but also highlighted the method's reliability and potential for scale-up in peptide synthesis. The structure of the final product was confirmed through Electrospray Ionization Mass Spectrometry (ESI-MS; see Supporting Information) and Nuclear Magnetic Resonance (NMR) analysis. After the synthesis, compound 3 was assayed for its binding to BSA, a model protein commonly used to evaluate the potential of new drug candidates to interact with serum albumins, which is relevant for their transport in the bloodstream [76]. To this end, we employed circular dichroism spectroscopy, recording the CD spectra of BSA alone and in the presence of compound 3. The intrinsic CD signal of compound 3 was recorded separately and then subtracted from the combined spectra in order to isolate the effects on BSA. Visual inspection of the resulting CD spectra (Fig. 1) indicates a clear interaction between the peptide and BSA, particularly in the 210–222 nm region. In this range, a noticeable decrease in CD intensity was shown at both characteristic minima, suggesting significant alterations in the secondary structure of BSA upon binding of compound 3.

For more quantitative information, we performed CD deconvolution of the spectra using the K2D2 program (see section 2.2).

The effect of compound 3 on BSA's secondary structure is moderate but clearly noticeable. The α-helix content decreases by about 7 percentage points (from 67.4% to 60.27%, Table 1), and the β-strand content shows a slight increase. Correspondingly, the CD minima at 210 and 222 nm display a reduced negative ellipticity, indicating partial destabilization of the α-helical structure. More in detail, the CD signal at 210 nm changes from −7.287 to −7.069 mdeg, and at 222 nm from −8.151 to −6.663 mdeg. This reduction in magnitude suggests a partial loss or destabilization of the α-helical structure in BSA induced by compound 3. Correspondingly, the predicted α-helix content decreases and, the predicted β-strand content increases from 2.2% to 4.79%, implying a possible slight shift toward β-structure formation (Table 1). Despite this moderate structural perturbation, BSA retains much of its native conformation and, therefore, likely its functional capacity. This suggests that BSA can still effectively perform its role as a transport protein for compound 3, supporting the potential of this drug to be carried without major loss of serum albumin function. Given the possible modulatory role of compound 3 in attenuating the antimicrobial activity of plant extracts, particularly in the gut, its binding to serum albumins may play a pivotal role in ensuring controlled systemic availability, stability, and co-localization with plant-derived compounds. Whether administered concurrently or as a pre-treatment, such transport mechanisms could be essential for achieving targeted and balanced modulation of microbiota-associated effects.

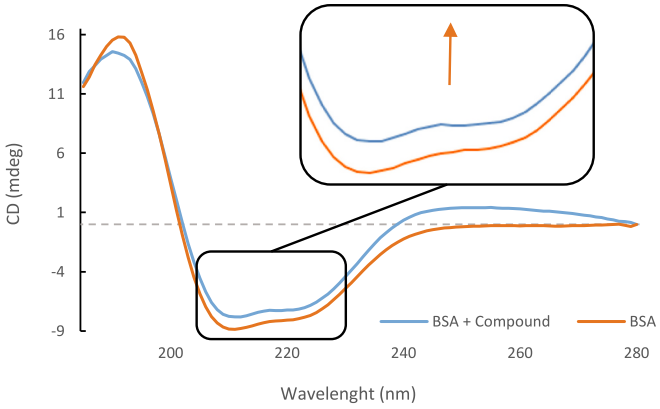
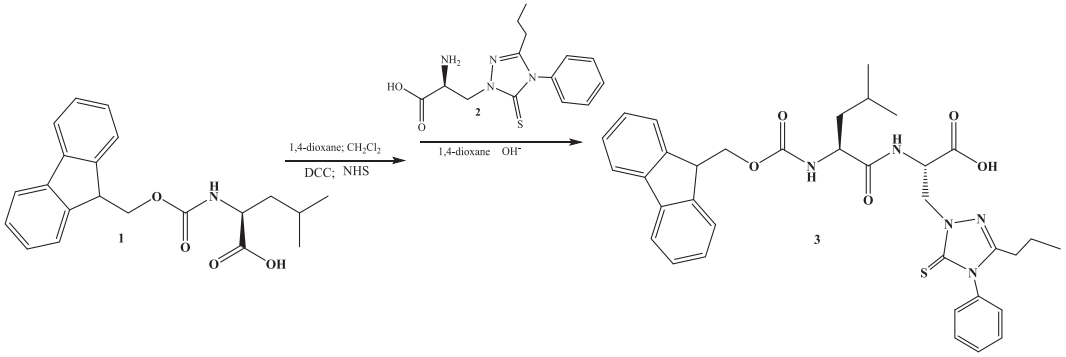


Fig. 1. CD analysis of the interaction between compound 3 and bovine serum albumin (BSA, 0.12 μM, phosphate buffer: pH of 7.4, 15 0C).



Scheme 1. Schematic representation of the synthetic route to the dipeptide 3.

Table 1
Circular Dichroism (CD) measurements at the characteristic α-helix minima (~210 nm and ~ 222 nm) and predicted secondary structure content of BSA samples with and without compound 3.

Sample	CD at 210 nm (mdeg)	CD at 222 nm (mdeg)	Predicted α-helix (%)	Predicted β-strand (%)
BSA only	−7.28702	−8.15085	67.4	2.2
BSA + 3	−7.0685	−6.66326	60.27	4.79

3.2. Antioxidant and antimicrobial studies of 3 combined with extracts of *Paeonia daurica*

The antioxidant properties of compound 3 were investigated using two complementary in vitro assays: the DPPH radical scavenging test and the TAC assay based on the phosphomolybdate method (Fig. 2). These approaches provided insight into the compound's ability to counteract free radicals and mitigate oxidative stress.

In the DPPH assay, dipeptide 3 demonstrated greater antioxidant activity when dissolved in methanol compared to DMSO. At a concentration of 500 μg/mL, the methanolic solution showed the highest activity (12.21%), whereas the same concentration in DMSO yielded a significantly lower value (7.44%). The IC_{50} for the methanol-based solution was also lower (2.39 ± 0.24 μg/mL) than that for the DMSO-based solution (2.84 ± 0.29 μg/mL), as shown in Fig. 2A and B.

Conversely, results from the phosphomolybdate-based TAC assay revealed an opposite trend. The DMSO solution of dipeptide 3 exhibited a higher total antioxidant capacity than its methanol counterpart. Specifically, at 450 μg/mL, the TAC value reached 29.10 ± 1.86 μg/mL AAE in DMSO, compared to 18.90 ± 0.96 μg/mL AAE in methanol (Fig. 2C and D). These findings suggest that solvent choice significantly influences the antioxidant performance of dipeptide 3, depending on the assay employed.

These contrasting results likely arise from differences in the peptide's solubility and structural behavior in the two solvents. The Fmoc group increases the peptide's lipophilicity, promoting better solubility in DMSO, which in turn enhances its reducing ability measured by the phosphomolybdate assay. Conversely, methanol's higher polarity and protic nature favor radical scavenging reactions in the DPPH assay but may limit peptide solubility and thus reduce the compound's overall antioxidant activity in the TAC assay. This shows how solvent-dependent interactions critically affect the peptide's found antioxidant capacity and confirms that the peptide's performance as an antioxidant is not solely determined by its inherent chemical properties but also due to the environment in which the compound is dissolved.

As part of a preliminary investigation, the antibacterial properties of dipeptide 3 were evaluated against *Escherichia coli* (*E. coli*), a widely used Gram-negative bacterial model. Specifically, its in vitro activity was assessed using disk diffusion assays, which measure bacterial growth inhibition based on the presence or absence of a clear zone

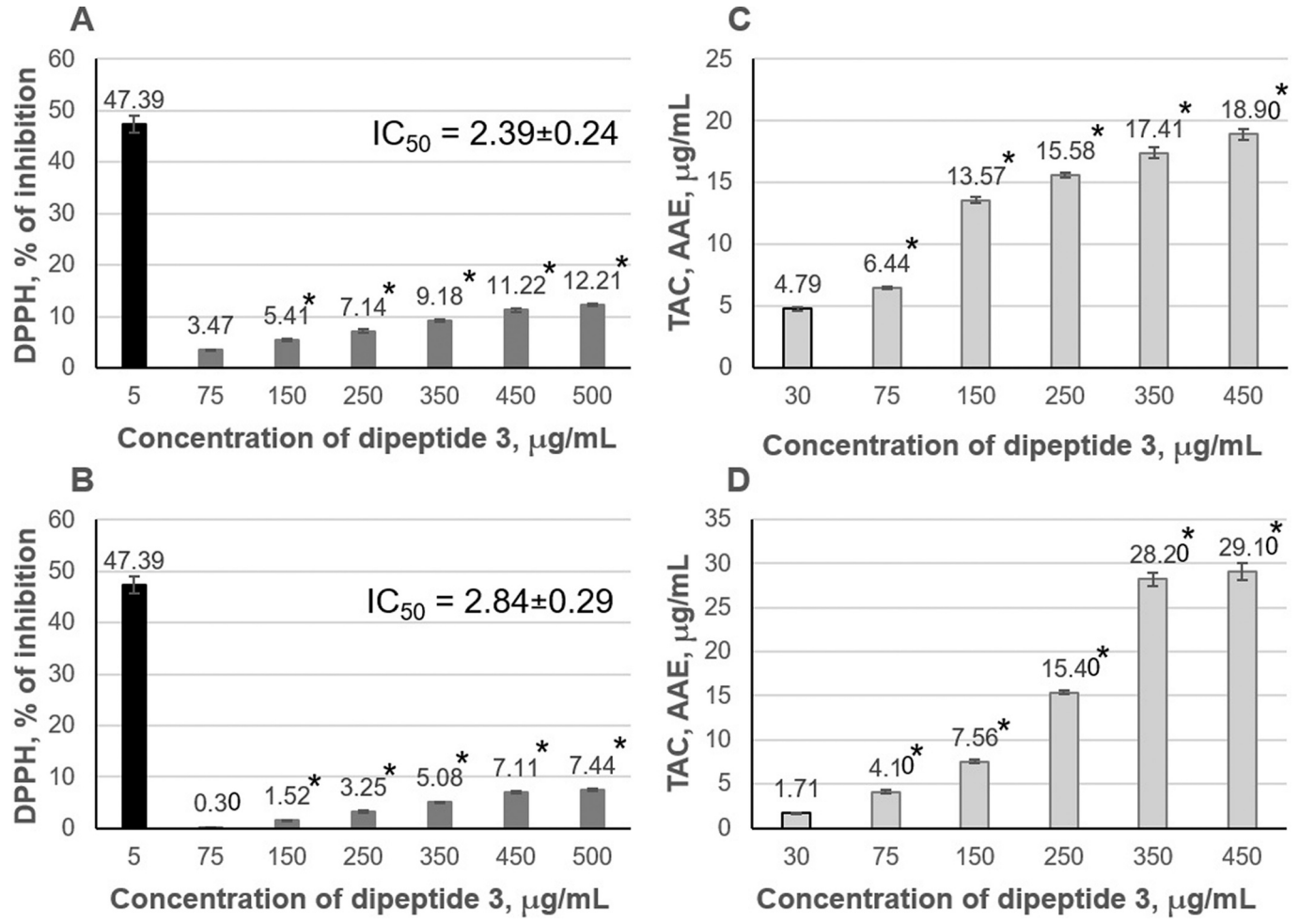


Fig. 2. In vitro assessment of the antioxidant potential of dipeptide 3, performed using DPPH (A and B) and total antioxidant capacity (TAC) assays (C and D). Panels A and C show results for dipeptide 3 dissolved in methanol, while panels B and D correspond to the DMSO-based solution. The black column represents a 5 μg/mL solution of ascorbic acid, used as a reference standard. Data are presented as mean ± standard deviation from three independent replicates. Asterisks indicate statistically significant differences (*$p < 0.05$, *t*-test) relative to the lowest tested concentration of dipeptide 3 within each respective assay.

surrounding the disk. Notably, dipeptide 3 did not exhibit any inhibitory effect on *E. coli* growth at concentrations ranging from 5 to 50 μg per disk (Fig. 3A). However, dipeptide 3 appeared to modulate the antibacterial efficacy of *Paeonia daurica* leaf and root extracts against *E. coli*, as illustrated in Fig. 3B and detailed in Table 2. When combined with the leaf extract, increasing amounts of dipeptide 3 led to a reduction in antibacterial activity, evidenced by a decrease in the inhibition zone (IZ) from 13.61 ± 0.17 mm for 200 μg/disk of leaf extract alone to 12.07 ± 0.15 mm when supplemented with 25 μg/disk of dipeptide 3 (Fig. 3B, disks 1–3). A similar trend was observed with the root extract: the IZ diminished from 13.75 ± 0.05 mm for 200 μg/disk of root extract to 10.20 ± 0.20 mm upon addition of 25 μg/disk of dipeptide 3 (Fig. 3B, disks 4–6 and Table 2). These findings suggest that specific interactions between dipeptide 3 and components of the extract matrix may influence antibacterial performance, warranting further investigation to elucidate the underlying mechanisms.

We hypothesize that when combined with the *Paeonia daurica* leaf or root extracts, dipeptide 3 likely interferes with the solubility and bioactivity of the active compounds in the extracts. The peptide's structural properties, including its lipophilicity and potential for complexation, might modulate the bioavailability of these antimicrobial compounds. This could also involve a modification of how the bioactive compounds from the extracts interact with bacterial targets, such as bacterial membranes or enzymes.

Our findings suggest that while the peptide does not directly inhibit bacterial growth, it could be modifying the effectiveness of plant-derived antimicrobial agents. The observed attenuation of antimicrobial activity by dipeptide 3 should not be viewed as a limitation, but rather as a strategically-relevant interaction. Our preliminary antimicrobial results highlight how sulfur-containing aromatic dipeptides can be used to modulate the complex bioactivity of plant extracts, potentially enabling safer, more precise, and multifunctional therapeutic strategies, with our approach supporting innovation in phytomedicine, particularly in developing combinatorial therapies that balance efficacy with safety.

3.3. Computational studies

3.3.1. Docking simulations involving the BSA interaction with peptide 3

Molecular docking studies conducted using the HDOCK platform [77] demonstrated a favorable binding affinity between compound 3 and bovine serum albumin (BSA; PDB ID: 4F5S) [78], occupying a cavity within chain B of the BSA dimer (Fig. 4a). The interaction is stabilized by both hydrophobic contacts and hydrogen bonds. Notably, hydrogen bonding occurs with residues Val342 and Gln220, while hydrophobic interactions involve residues Arg194 and Ala290 (see Fig. 4b).

The top-ranked docking pose of compound 3 demonstrated a favorable binding affinity to the serum albumin target, with an HDOCK score of −152.24 (Table 3).

The average score of the top three models (−146.12 ± 5.36) further supports a consistent and stable interaction. In the best-scoring pose, compound 3 engages with Arg194, Gln220, Val342, and Ala290 through hydrophobic contacts and hydrogen bonding, at distances ranging from 2.40 to 3.09 Å (Table 3).

Overall, our docking results are consistent with the CD findings, which indicate a moderate but clear effect of compound 3 on bovine serum albumin's secondary structure. The binding of 3, localized within a cavity of chain B and stabilized by specific hydrogen bonds and hydrophobic contacts, likely induces subtle conformational changes, reflected in the decreased alpha-helical content and reduced negative ellipticity at 210 and 222 nm. This partial destabilization of the alpha-helix suggests a ligand-induced structural adjustment rather than

Table 2
Antibacterial activity of different concentrations of compound 3 and *Paeonia* leaf and root extracts against *Escherichia coli*. Asterisks refer to significant differences (*t*-test, * $p < 0.05$) when compared to the antibacterial activity of the corresponding *Paeonia* extracts without dipeptide 3. nd – not detected.

Concentration of dipeptide 3	*Paeonia daurica* extract (organ/concentration)	Inhibition zone (IZ), mm (mean ± SD)
5–50 μg/disk	nd	nd
0	Leaf/200 μg/disk	13.61 ± 0.17
12 μg/disk	Leaf/200 μg/disk	12.53 ± 0.15*
25 μg/disk	Leaf/200 μg/disk	12.07 ± 0.15*
0	Root/200 μg/disk	13.75 ± 0.05
12 μg/disk	Root/200 μg/disk	11.47 ± 0.31*
25 μg/disk	Root/200 μg/disk	10.20 ± 0.20*

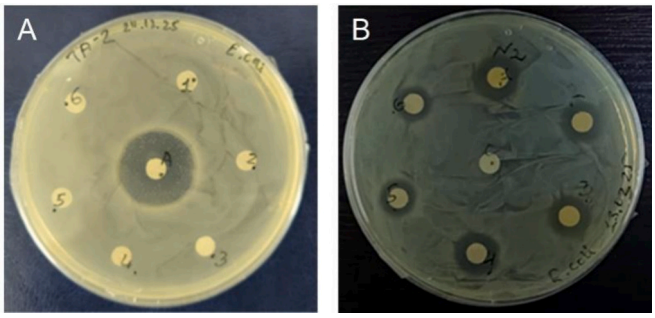


Fig. 3. Zones of inhibition of different concentrations of 3 and *Paeonia* leaf and root extracts against *Escherichia coli*. A. 1 – dipeptide 3 5 μg/disk; 2 - dipeptide 3 10 μg/disk; 3 - dipeptide 3 15 μg/disk; 4 - dipeptide 3 25 μg/disk; 5 - dipeptide 3 40 μg/disk; 6 – dipeptide 3 50 μg/disk, A – positive control, 30 μg/disk Amoxicillin. B. 1 - *Paeonia* leaf extract 200 μg/disk; 2 - *Paeonia* leaf extract 200 μg/disk + dipeptide 3 12 μg/disk; 3 - *Paeonia* leaf extract 200 μg/disk + dipeptide 3 25 μg/disk; 4 - *Paeonia* root extract 200 μg/disk; 5 - *Paeonia* root extract 200 μg/disk + dipeptide 3 12 μg/disk; 6 - *Paeonia* root extract 200 μg/disk + dipeptide 3 25 μg/disk. C – negative control, 10 μL/disk 80% DMSO.

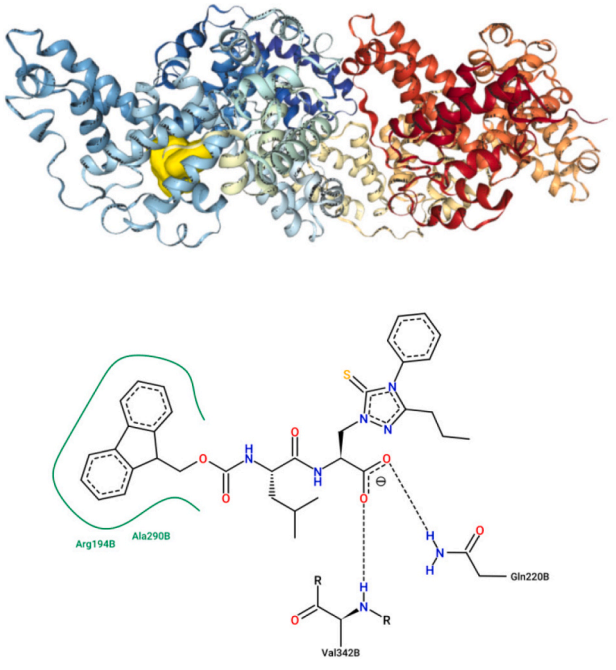


Fig. 4. Molecular docking analysis carried out using bovine serum albumin (BSA, PDB ID: 4F5S) and compound 3. (a) The top-ranked binding conformation (Top-1) is depicted, with the dipeptide ligand highlighted in yellow for visual emphasis. (b) A schematic representation of molecular interactions was generated via ProteinPlus (https://proteins.plus/, accessed on 7 April 2025), illustrating key contacts between the ligand and protein residues. (For interpretation of the references to colour in this figure legend, the reader is referred to the web version of this article.)

Table 3
HDOCK scores (Top1 and means of the Top1–3 scores ±S.D.) predicted for the formation of the complex of 3 with BSA, interacting residues in the Top 1 pose, and corresponding interaction distances (Å).

Top-1 Binding energy (HDOCK Score)	Average binding energy (Top 1–3)	Standard deviation (Top 1–3)	Key interacting residues in Top-1 pose	Interaction distances (Å)
−152.24	−146.12	5.36	Arg194, Gln220, Val342, Ala290	Arg194–Ligand: 2.40 Gln220–Ligand: 2.66 Val342–Ligand: 3.09 Ala290–Ligand: 2.69

complete unfolding, indicating that bovine serum albumin remains functionally capable of transporting compound 3 while accommodating its binding.

3.3.2. *DFT-based computational analysis*

To better understand the electronic structure, reactivity, and antioxidant mechanism of 3, DFT calculations were performed under different conditions. More in detail, equilibrium geometries (see output coordinates in the Supporting Information) were evaluated in the gas phase as well as under MeOH and DMSO solvation conditions. A strong similarity was observed between the geometries optimized in DMSO and MeOH. As shown by theRMSD values in Fig. 5, these latter structures are nearly identical, with only minor deviations compared to the gas-phase geometry. MEP maps (Fig. 6a–h) reveal a generally homogeneous charge distribution across the molecular surfaces, except in the region surrounding the sulfur atom, which exhibits electron-rich lone pairs. This consistent charge distribution across the three optimization conditions is attributed to the similar structures. Additionally, a hydrogen bond is present between the benzyl substituent of the thioxo-triazole ring and the fluorene group, measuring 2.65 Å in solvation condition. This interaction helps to stabilize the structure in all examined conditions. From a biological perspective, polarized groups are known to interact effectively with cell membranes, while the presence of fluorene and aliphatic groups may enhance membrane permeability. Due to the absence of highly polarized groups on the molecular surface, which are consistent with a uniform MEP distribution, no significant structural modifications are observed for the peptide across different conditions. Despite the molecule's high dipole moment values (see Table 4), the estimated Log(P) value of 6.52 suggests that an active transporter may be required for uptake in the cells, which will be likely necessary to prevent the entrapment of this lipophilic dipeptide within membrane layers and to improve its absorption by cells [79,80]. FMOs provide insights into the molecule's reactivity and its interaction with Reactive Oxygen Species (ROS) [66,70]. In this context, the HOMO represents the region or functional group of the peptide which donate an electron most likely during interactions with scavengers, whereas the LUMO indicates the area where molecular reduction is more probable. The dipeptide's FMOs (see Fig. 7a–e) were calculated in the gas phase, MeOH, and DMSO solvation conditions, and energy gaps are reported in Table 4. As depicted in Fig. 7c, the HOMO is localized on the thioxo-triazole moiety, where the highest spin density (triplet state) is also observed (Fig. 7e).

This suggests that electron scavenging by ROS, including DPPH in this case, likely occurs on this ring. Conversely, the LUMO is mainly distributed over the fluorene group, likely due to its extended conjugation, which effectively stabilizes a negative charge upon reduction. The FMOs maintain their spatial distribution in both the gas phase and in the two solvents, with the calculated energy gaps remaining consistent across all three conditions. This observation indicates that the HOMO/LUMO gaps in the gas phase, MeOH, and DMSO are virtually identical. To further explore the antioxidant mechanism with DPPH, we hypothesized that the thioxo-triazole ring, where the HOMO is primarily located, serves as site for the SET process. IPs were evaluated to understand this oxidation pathway. As shown in Table 4, no significant differences were found between the IPs in either solvent, as well as in the corresponding FMO energy gaps suggesting similar antioxidant capacity. However, experimental results indicate a higher RSA% in MeOH, thus we assumed that this discrepancy is caused by the potential radical-scavenging nature of DMSO, which may lead to an experimental underestimation of RSA%, although IPs energies are similar. In the context of TAC assays, an inversion in the trend of activity was observed in our study, with higher antioxidant activity detected in DMSO compared to MeOH. To investigate this experimental outcome, additional computational analysis was performed on the oxidation of the thioxo-triazole ring by ammonium phosphomolybdate, which is able to oxidize the ring generating a zwitterionic species, as illustrated in Fig. 8. For this purpose, we calculated the formation enthalpy of the oxidized product – reported as $BFE_{N\text{-}O}$ – as detailed in the Methods section. As shown in Table 4, the formation enthalpy is slightly more favorable in DMSO than in MeOH, aligning with the experimental observations. This suggests that thermodynamic factors may partially explain the observed trend inversion. Additional contributing factors may include solvent effects, such as improved solubilization and stabilization of the transition state leading to N^{+}-O^{-} bond formation, particularly considering the significantly higher dielectric constant of DMSO compared to MeOH.

TD-SCF calculation predicted the UV–vis spectrum (Fig. S6), identifying a singlet-state absorption at a wavelength of 258 nm (4.79 eV, f = 0.29). This peak is attributed to an $n \rightarrow \pi^*$ transition from the sulfur lone pair to the fluorene group, involving an electronic transition between $HOMO^{-1}$ (169) and LUMO (171) with a 57% contribution. Another absorption was observed at 240 nm (5.15 eV, f = 0.15), generated by electronic transitions from the HOMO (170) to higher molecular orbitals with varying contributions. When compared with the experimental UV–vis spectrum in MeOH, the 263 nm absorption peak is assigned to the transition between the sulfur lone pair and the fluorene group, while the 237 nm absorption is linked to the thioxo-triazole transition. Overall, the computational studies employed in our work not only provided insight into the binding mode of the sulfur-containing dipeptide toward

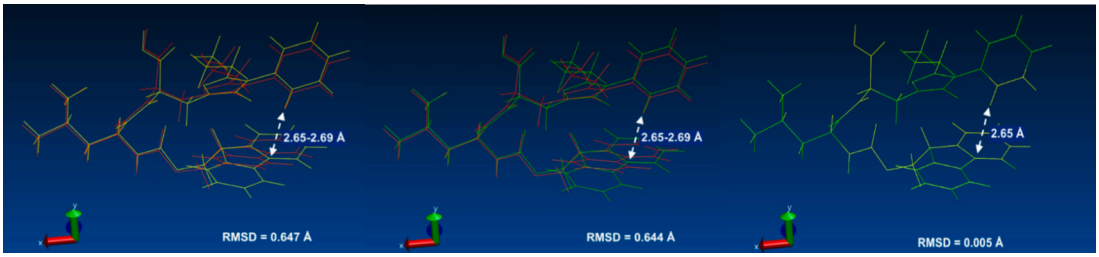


Fig. 5. Superimposition of structures depicted with different colour and RMSD values respectively. White arrows represent the CH-π hydrogen bond length. Red molecule: gas phase. Green molecule: MeOH. Yellow molecule: DMSO. (For interpretation of the references to colour in this figure legend, the reader is referred to the web version of this article.)

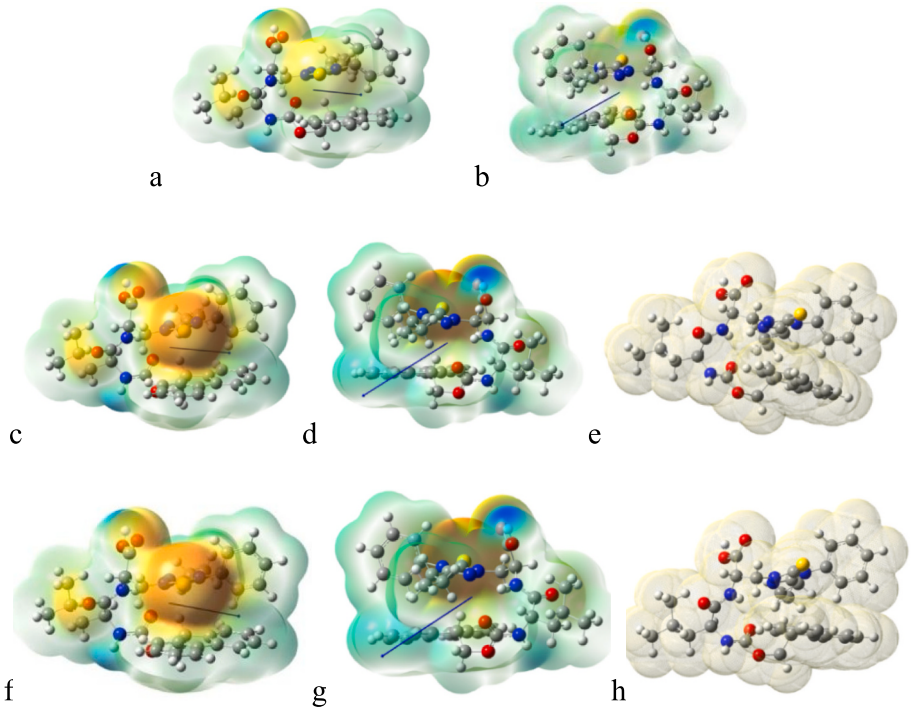


Fig. 6. MEPs and dipole moment vectors of the dipeptide on the front (a) and on the back (b) side in gas phase. Front side (c), back side (d), and solvation sphere (e) in MeOH. Front side (f), back side (g), and solvation sphere (h) in DMSO. MEPs charge scale were normalized at the same range.

Table 4
HOMO/LUMO gaps, dipole moments, ionization energies and $BFE_{N\text{-}O}$ for TAC interpretation calculated in gas phase, MeOH and DMSO at ωB97XD/6-31+g(d,p) level of theory.

ωB97XD/ 6-31+g(d,p)	Dipole moment (D)	HOMO/LUMO gap (eV)	HOMO/LUMO gap $\left(\frac{kcal}{mol}\right)$	IP (eV)	IP $\left(\frac{kcal}{mol}\right)$	$BFE_{N\text{-}O}$ (eV)	$BFE_{N\text{-}O}$ $\left(\frac{kcal}{mol}\right)$
Gas phase	6.51	6.89	159	6.95	160	−4.93	−114
MeOH	10.2	6.91	159	6.00	138	−4.21	−97.1
DMSO	10.2	6.87	158	6.01	138	−4.85	−112

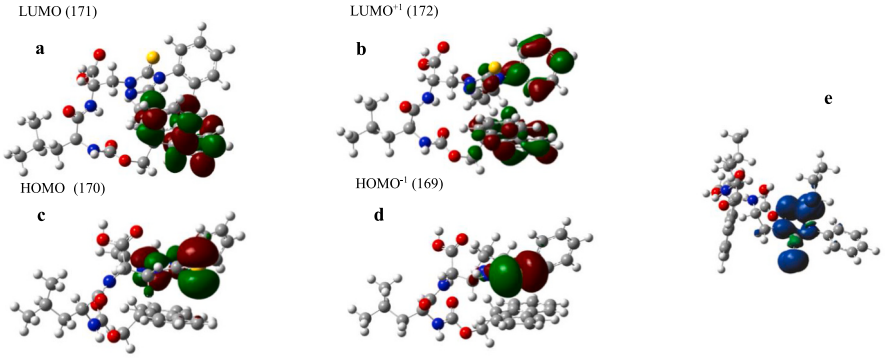


Fig. 7. FMOs depictions (a,b,c,d) and triplet state spin density (e). Those present the HOMO localized on the thioxo-triazole ring which is involved in the oxidation, while the reduction takes place on the fluorene group (LUMO). HOMO-1 is involved in the $n \rightarrow \pi^*$ transition at 263 nm.

the BSA protein, but also offered a plausible explanation for the antioxidant behavior of this synthetic derivative. These findings further highlight the current relevance and impact of computational chemistry in medicinal chemistry and drug discovery [81–84].

4. Conclusions

The sulfur-containing aromatic dipeptide 3 exhibits notable antioxidant activity, with solvent-dependent efficiency demonstrated by both DPPH radical scavenging and total antioxidant capacity assays. While 3 itself showed no direct antibacterial activity, its combination with methanolic extracts of the Caucasus plant *Paeonia daurica* subsp. *mlokosewitschii* resulted in a dose-dependent reduction of the plant's antimicrobial efficacy, suggesting a modulatory interaction. *Paeonia daurica* extracts demonstrated measurable antibacterial activity against *E. coli* in the absence of dipeptide 3. At a concentration of 200 μg/disk, the leaf extract produced an inhibition zone of 13.61 ± 0.17 mm, while the root extract resulted in a slightly larger zone of 13.75 ± 0.05 mm. Although

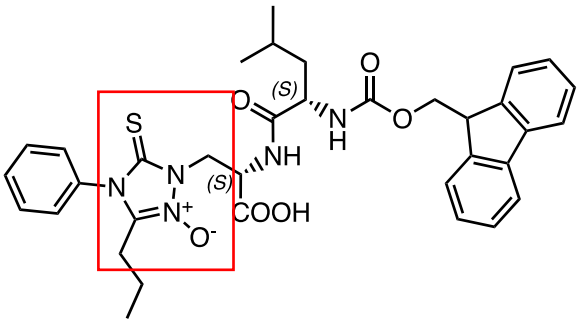


Fig. 8. Thioxo-triazole ring oxidized derivative by phosphomolybdate assay (TAC).

the dipeptide alone exhibited no antibacterial activity, its combination with methanolic extracts of *Paeonia daurica* subsp. *mlokosewitschii* produced a dose-dependent attenuation of the plant's antimicrobial efficacy, without fully abolishing it, suggesting a modulatory role. This suggests that sulfur-containing aromatic dipeptides may mitigate the impact of antimicrobial plant extracts on the human gut microbiome while preserving their antibacterial potential. Peptide 3's properties, such as its short length, limited positive charge, and insufficient amphipathicity, are likely responsible for its lack of antimicrobial activity and reduced solubility. However, it still maintains notable antioxidant and protein-binding capabilities. Circular dichroism studies including CD deconvolution (Fig. S7) and computational modeling confirmed the dipeptide's ability to interact with both hydrophobic and polar residues of serum proteins, supporting its potential biological role and capacity for transport in the bloodstream. Computational evaluation via DFT supported the experimental findings, revealing similar energy gaps in DMSO and MeOH; however, DMSO exhibited a lower RSA% due to its intrinsic radical-scavenging properties. FMO analysis identified the thioxo-triazole ring as the primary site of oxidation, occurring through a SET mechanism. MEP maps provided insights into the peptide's membrane permeability and suggested the potential need for an active transporter to facilitate cellular uptake. Interestingly, an inversion of results was observed in the TAC assay, attributed to a thermodynamic factor. Additionally, the UV–Vis spectrum predicted by TD-SCF aligned well with the experimental data. These findings highlight compound 3 as a bioactive molecule of interest in the context of phytotherapy research, particularly for its antioxidant properties and its capacity to modulate the bioactivity of natural plant extracts. More broadly, sulfur-containing aromatic dipeptides could serve as modulatory agents that attenuate the antimicrobial potency of plant extracts. This attenuation may contribute to preserving beneficial components of the human microbiome and mitigating potential toxicity associated with overly potent plant-based therapies, as several plant extracts have been shown to exert inhibitory effects on the human gut microbiome [23]. To our knowledge, this is among the first studies to explore such interactions, offering a novel strategy for balancing efficacy and safety in phytotherapy-based treatments. Compound 3's ability to interact with serum proteins, which facilitate its transport in the bloodstream, and its antioxidant properties make it a promising candidate as a peptide additive in herbal medicine formulations. Further investigation into its biological interactions and in vivo efficacy will be essential to fully harness its potential in complementary and integrative medicine.

CRediT authorship contribution statement

Tatevik Sargsyan: Methodology, Investigation, Data curation. **Silva Jamgaryan:** Investigation, Formal analysis. **Lala Stepanyan:** Methodology, Investigation. **Avetis Tsaturyan:** Writing – original draft, Methodology. **Valentina Mittova:** Writing – original draft, Methodology, Investigation. **Zurab R. Tsetskhladze:** Methodology, Formal analysis, Data curation. **Nino Motsonelidze:** Methodology, Formal analysis. **Ekaterine Gorgoshidze:** Methodology, Investigation. **Niccolò Nova:** Methodology, Investigation. **Hayarpi Simonyan:** Methodology, Investigation. **Karapet Ghazaryan:** Methodology, Investigation. **Franco Bisceglie:** Methodology, Investigation. **Giovanni N. Roviello:** Writing – original draft, Supervision, Methodology, Investigation, Conceptualization.

Declaration of competing interest

The authors declare that they have no known competing financial interests or personal relationships that could have appeared to influence the work reported in this paper.

Acknowledgements

The authors gratefully acknowledge the High-Performance Computing (HPC) facility at the University of Parma, Italy, and Prof. Francesco Di Maiolo for his valuable guidance and technical support. This research has drawn upon resources and infrastructure provided by the COMPHUB and COMP-R Initiatives, supported by the 'Departments of Excellence' program of the Italian Ministry for University and Research (MIUR, 2018–2022; MUR, 2023–2027). Additional funding was provided by the Higher Education and Science Committee of the Ministry of Education, Science, Culture and Sports of the Republic of Armenia (MESCS RA), under project number 24RL-1D014.

Appendix A. Supplementary data

Supplementary data to this article can be found online at https://doi.org/10.1016/j.rechem.2026.103214.

Data availability

Data will be made available on request.

References

[1] T. Sang, D.J. Crawford, T.F. Stuessy, Chloroplast DNA phylogeny, reticulate evolution, and biogeography of Paeonia (Paeoniaceae), Am. J. Bot. 84 (8) (1997) 1120–1136, https://doi.org/10.2307/2446155.
[2] X. Zhang, Y. Zhai, J. Yuan, et al., New insights into Paeoniaceae used as medicinal plants in China, Sci. Rep. 9 (2019) 18469, https://doi.org/10.1038/s41598-019-54863-y.
[3] Paeonia mlokosewitschii, in: N. Ketskhoveli (Ed.), Flora of Georgia, 2nd ed. II, Metsniereba, Tbilisi, Georgia, 1973, pp. 8–15.
[4] T. Nadiradze, N. Eradze, Overview of Paeonia mlokosewitschii L, World J Adv Res Rev. 6 (2) (2020) 5–8, https://doi.org/10.30574/wjarr.2020.6.2.0113.
[5] G. Demirboğa, Y. Demirboğa, N. Özbay, Types of Paeonia and their use in phytotherapy, Karadeniz Fen Bilimleri Dergisi. 11 (1) (2021) 318–327, https://doi.org/10.31466/kfbd.835385.
[6] G.N. Roviello, V. Mittova, Z.R. Tsetskhladze, et al., Antioxidant properties of Some Caucasian medicinal plants, MIMM 27 (1) (2024), https://doi.org/10.56580/GEOMEDI44.
[7] S. Nakamura, Y. Mukudai, J. Chikuda, M. Zhang, H. Shigemori, K. Yazawa, S. Kondo, T. Shimane, T. Shirota, Combinational anti-tumor effects of chemicals from Paeonia lutea leaf extract in Oral squamous cell carcinoma cells, Anticancer Res. 41 (12) (2021) 6077–6086, https://doi.org/10.21873/anticanres.
[8] E. Yesilada, A. Mutlugil, B. Sener, The antiinflammatory principle of the roots of Paeonia daurica, Int. J. Pharmacogn. 30 (1) (1992) 66–70, https://doi.org/10.3109/13880209209054635.
[9] M. Ajvazi, I. Osmani, D. Gashi, E. Krasniqi, L. Zeneli, Radical Scavenging, Antioxidant and Antimicrobial Activity of Paeonia Peregrina Mill., *Paeonia mascula (L.)* Mill. and *Paeonia officinalis (L.)*, Iran. J. Chem. Chem. Eng. 42 (2023) 3835–3848, https://doi.org/10.30492/ijcce.2023.1978423.5755.
[10] N.N. Tong, X.Y. Zhou, L.P. Peng, Z.A. Liu, Q.Y. Shu, A comprehensive study of three species of Paeonia stem and leaf phytochemicals, and their antioxidant activities, J. Ethnopharmacol. 12 (273) (2021) 113985, https://doi.org/10.1016/j.jep.2021.113985.
[11] A. Ivanova, I. Delcheva, I. Tsvetkova, A. Kujumgiev, I. Kostova, GC-MS analysis and anti-microbial activity of acidic fractions obtained from Paeonia peregrina and Paeonia tenuifolia roots, Z. Naturforsch. C 57 (7–8) (2002) 624–628, https://doi.org/10.1515/znc-2002-7-813.

[12] P. Li, J. Shen, Z. Wang, S. Liu, Q. Liu, Y. Li, C. He, P. Xiao, Genus Paeonia: a comprehensive review on traditional uses, phytochemistry, pharmacological activities, clinical application, and toxicology, J. Ethnopharmacol. 269 (2021) 113708, https://doi.org/10.1016/j.jep.2020.113708.
[13] M.A. Fik-Jaskółka, A.F. Mkrtchyan, A.S. Saghyan, R. Palumbo, A. Belter, L. A. Hayriyan, H. Simonyan, V. Roviello, G.N. Roviello, Spectroscopic and SEM evidences for G4-DNA binding by a synthetic alkyne-containing amino acid with anticancer activity, Spectrochim. Acta A Mol. Biomol. Spectrosc. 229 (2020) 117884, https://doi.org/10.1016/j.saa.2019.117884.
[14] V. Roviello, D. Musumeci, A. Mokhir, G.N. Roviello, Evidence of protein binding by a nucleopeptide based on a thymine-decorated L-diaminopropanoic acid through CD and in silico studies, Curr. Med. Chem. 28 (24) (2021) 5004–5015, https://doi.org/10.2174/0929867328666210201152326.
[15] M. Marzano, A.P. Falanga, D. Marasco, N. Borbone, S. D'Errico, G. Piccialli, G. N. Roviello, G. Oliviero, Evaluation of an analogue of the marine ε-PLL peptide as a ligand of G-quadruplex DNA structures, Mar. Drugs 18 (1) (2020) 49, https://doi.org/10.3390/md18010049.
[16] G.N. Roviello, A. Ricci, E.M. Bucci, C. Pedone, Synthesis, biological evaluation and supramolecular assembly of novel analogues of peptidyl nucleosides, Mol. BioSyst. 7 (2011) 1773–1778, https://doi.org/10.1039/C1MB05007A.
[17] G.N. Roviello, A. Ricci, E.M. Bucci, C. Pedone, Evidences for supramolecular organization of nucleopeptides, Mol. BioSyst. 5 (2011) 1773, https://doi.org/10.1039/C0MB00214C.
[18] G.N. Roviello, D. Musumeci, C. Pedone, E.M. Bucci, Synthesis, characterization and hybridization studies of an alternate nucleo-ε/γ-peptide: complexes formation with natural nucleic acids, Amino Acids 38 (1) (2010) 103–111, https://doi.org/10.1007/s00726-008-0214-7.
[19] D. Musumeci, G. Oliviero, G.N. Roviello, E.M. Bucci, G. Piccialli, G-quadruplex-forming oligonucleotide conjugated to magnetic nanoparticles: synthesis, characterization, and enzymatic stability assays, Bioconjug. Chem. 23 (3) (2012) 382–391, https://doi.org/10.1021/bc200305t.
[20] H. Simonyan, R. Palumbo, C. Vicidomini, P.L. Scognamiglio, S. Petrosyan, L. Sahakyan, G. Melikyan, A. Saghyan, G.N. Roviello, Binding of G-quadruplex DNA and serum albumins by synthetic non-proteinogenic amino acids: implications for c-Myc-related anticancer activity and drug delivery, Mol Ther Nucleic Acids. 36 (2) (2025) 102478, https://doi.org/10.1016/j.omtn.2025.102478.
[21] T. Sargsyan, L. Stepanyan, H. Panosyan, H. Hakobyan, M. Israyelyan, A. Tsaturyan, N. Hovhannisyan, C. Vicidomini, A. Mkrtchyan, A. Saghyan, et al., Synthesis and antifungal activity of Fmoc-protected 1,2,4-triazolyl-α-amino acids and their dipeptides against aspergillus species, Biomolecules 15 (1) (2025) 61, https://doi.org/10.3390/biom15010061.
[22] M.J. Cheesman, A. Ilanko, B. Blonk, I.E. Cock, Developing new antimicrobial therapies: are synergistic combinations of plant extracts/compounds with conventional antibiotics the solution? Pharmacogn. Rev. 11 (22) (2017) 57–72, https://doi.org/10.4103/phrev.phrev_21_17.
[23] S. Pérez-Burillo, D. Hinojosa-Nogueira, S. Pastoriza, J.A. Rufián-Henares, Plant extracts as natural modulators of gut microbiota community structure and functionality, Heliyon 6 (11) (2020) e05474, https://doi.org/10.1016/j.heliyon.2020.e05474.
[24] K.H. Min, K.H. Kim, M.R. Ki, S.P. Pack, Antimicrobial peptides and their biomedical applications: a review, Antibiotics 13 (2024) 794, https://doi.org/10.3390/antibiotics13090794.
[25] A. Mulukutla, R. Shreshtha, V. Kumar Deb, P. Chatterjee, U. Jain, N. Chauhan, Recent advances in antimicrobial peptide-based therapy, Bioorg. Chem. 145 (2024) 107151, https://doi.org/10.1016/j.bioorg.2024.107151.
[26] M. Naeem, M.I. Malik, T. Umar, et al., A comprehensive review about bioactive peptides: sources to future perspective, Int. J. Pept. Res. Ther. 28 (2022) 155, https://doi.org/10.1007/s10989-022-10465-3.
[27] M. Akbarian, A. Khani, S. Eghbalpour, V.N. Uversky, Bioactive peptides: synthesis, sources, applications, and proposed mechanisms of action, Int. J. Mol. Sci. 23 (3) (2022) 1445, https://doi.org/10.3390/ijms23031445.
[28] A. Kasana, V. Verma, Food-derived bioactive peptides as potential antimicrobial agents: Challenges and opportunities, in: D. Lahiri, M. Nag, D. Bhattacharya, S. Pati, T. Sarkar (Eds.), Bioactive Ingredients for Healthcare Industry 2, Springer, Singapore, 2025, https://doi.org/10.1007/978-981-96-4379-0_8.
[29] Y. Zhu, K. Wang, X. Jia, C. Fu, H. Yu, Y. Wang, Antioxidant peptides, the guardian of life from oxidative stress, Med. Res. Rev. 43 (6) (2023) 1–28, https://doi.org/10.1002/med.21986.
[30] G. López-García, O. Dublan-García, D. Arizmendi-Cotero, L.M. Gómez Oliván, Antioxidant and antimicrobial peptides derived from food proteins, Molecules 27 (2022) 1343, https://doi.org/10.3390/molecules27041343.
[31] Y. Zhang, Y. Li, Z. Quan, P. Xiao, J.-A. Duan, New insights into antioxidant peptides: An overview of efficient screening, evaluation models, molecular mechanisms, and applications, Antioxidants 13 (2024) 203, https://doi.org/10.3390/antiox13020203.
[32] J. Fetse, S. Kandel, U.F. Mamani, K. Cheng, Recent advances in the development of therapeutic peptides, Trends Pharmacol. Sci. 44 (2023) 425–441, https://doi.org/10.1016/j.tips.2023.04.003.
[33] S. Chapagain, S. Ojha, S.P. Khanal, N.P. Adhikari, Thermodynamics properties of leucine and isoleucine peptides in water, ChemistryOpen 14 (1) (2025) e202400209, https://doi.org/10.1002/open.202400209.
[34] N.J. Gay, L.C. Packman, M.A. Weldon, J.C. Barna, A leucine-rich repeat peptide derived from the Drosophila toll receptor forms extended filaments with a beta-sheet structure, FEBS Lett. 291 (1) (1991) 87–91, https://doi.org/10.1016/0014-5793(91)81110-t.
[35] A. Gostaviceanu, S. Gavrilaş, L. Copolovici, D.M. Copolovici, Membrane-active peptides and their potential biomedical application, Pharmaceutics 15 (2023) 2091, https://doi.org/10.3390/pharmaceutics15082091.
[36] P. Kumar, J.N. Kizhakkedathu, S.K. Straus, Antimicrobial peptides: diversity, mechanism of action and strategies to improve the activity and biocompatibility in vivo, Biomolecules 8 (2018) 4, https://doi.org/10.3390/biom8010004.
[37] A.A. Zaky, J. Simal-Gandara, J.B. Eun, J.H. Shim, A.M. Abd El-Aty, Bioactivities, applications, safety, and health benefits of bioactive peptides from food and by-products: a review, Front. Nutr. 8 (2022) 815640, https://doi.org/10.3389/fnut.2021.815640.
[38] W. Dong, X. Zhu, X. Zhou, Y. Yang, X. Yan, L. Sun, D. Shang, Potential role of a series of lysine−/leucine-rich antimicrobial peptide in inhibiting lipopolysaccharide-induced inflammation, Biochem. J. 475 (22) (2018) 3687–3706, https://doi.org/10.1042/BCJ20180483.
[39] J.L. Hickey, D. Sindhikara, S.L. Zultanski, D.M. Schultz, Beyond 20 in the 21st century: prospects and challenges of non-canonical amino acids in peptide drug discovery, ACS Med. Chem. Lett. 14 (5) (2023) 557–565, https://doi.org/10.1021/acsmedchemlett.3c00037.
[40] Y. Ding, J.P. Ting, J. Liu, M. Al-Azzawi, A.N. Pandya, S. Afshar, Impact of non-proteinogenic amino acids in the discovery and development of peptide therapeutics, Amino Acids 52 (9) (2020) 1207–1226, https://doi.org/10.1007/s00726-020-02890-9.
[41] T. Baumann, J.H. Nickling, M. Bartholomae, A. Buivydas, O.P. Kuipers, N. Budisa, Prospects of in vivo incorporation of non-canonical amino acids for the chemical diversification of antimicrobial peptides, Front. Microbiol. 8 (2017) 124, https://doi.org/10.3389/fmicb.2017.00124.
[42] T.G. Castro, M. Melle-Franco, C.E.A. Sousa, A. Cavaco-Paulo, J.C. Marcos, Non-canonical amino acids as building blocks for peptidomimetics: structure, function, and applications, Biomolecules 13 (6) (2023) 981, https://doi.org/10.3390/biom13060981.
[43] J. Grabeck, J. Mayer, A. Miltz, M. Casoria, M. Quagliata, D. Meinberger, A.R. Klatt, I. Wielert, B. Maier, A.M. Papini, I. Neundorf, Triazole-bridged peptides with enhanced antimicrobial activity and potency against pathogenic bacteria, ACS Infect Dis. 10 (8) (2024) 2717–2727, https://doi.org/10.1021/acsinfecdis.4c00078.
[44] T. Sargsyan, L. Stepanyan, H. Panosyan, H. Hakobyan, M. Israyelyan, A. Tsaturyan, N. Hovhannisyan, C. Vicidomini, A. Mkrtchyan, A. Saghyan, G.N. Roviello, Synthesis and antifungal activity of Fmoc-protected 1,2,4-triazolyl-α-amino acids and their dipeptides against Aspergillus species, Biomolecules 15 (1) (2025) 61, https://doi.org/10.3390/biom15010061.
[45] E. Stingaci, M. Zveaghinteva, S. Pogrebnoi, L. Lupascu, V. Valica, L. Uncu, A. Smetanscaia, M. Drumea, A. Petrou, A. Ciric, J. Glamoclija, M. Sokovic, V. Kravtsov, A. Geronikaki, F. Macaev, New vinyl-1,2,4-triazole derivatives as antimicrobial agents: synthesis, biological evaluation and molecular docking studies, Bioorg. Med. Chem. Lett. 30 (17) (2020) 127368, https://doi.org/10.1016/j.bmcl.2020.127368.
[46] M. Staś, M.A. Broda, D. Siodłak, Thiazole-amino acids: influence of thiazole ring on conformational properties of amino acid residues, Amino Acids 53 (5) (2021) 673–686, https://doi.org/10.1007/s00726-021-02974-0.
[47] M. Krátký, J. Vinsová, Sulphur-containing heterocycles as antimycobacterial agents: recent advances in thiophene and thiadiazole derivatives, Curr. Top. Med. Chem. 16 (26) (2016) 2921–2952, https://doi.org/10.2174/1568026616666160506131118.
[48] Y. Liao, M. Wang, X. Jiang, Sulfur-containing peptides: synthesis and application in the discovery of potential drug candidates, Curr. Opin. Chem. Biol. 75 (2023) 102336, https://doi.org/10.1016/j.cbpa.2023.102336.
[49] A.S. Sargsyan, L.T. Karapetyan, A.V. Mkhitaryan, L.A. Stepanyan, T.H. Sargsyan, Y. M. Danghyan, A.V. Sargsyan, G.G. Oganezova, N.A. Hovhannisyan, Modeling, synthesis and in vitro testing of peptides based on unusual amino acids as potential antibacterial agents, Biomed. Khim. 70 (6) (2024) 413–420, https://doi.org/10.18097/PBMC20247006413.
[50] A. Staśkiewicz, P. Ledwoń, P. Rovero, A.M. Papini, R. Latajka, Triazole-modified peptidomimetics: an opportunity for drug discovery and development, Front. Chem. 9 (2021) 674705, https://doi.org/10.3389/fchem.2021.674705.
[51] R. Gattu, S.S. Ramesh, S. Nadigar, C.G. D, S. Ramesh, Conjugation as a tool in therapeutics: role of amino acids/peptides-bioactive (including heterocycles) hybrid molecules in treating infectious diseases, Antibiotics 12 (3) (2023) 532, https://doi.org/10.3390/antibiotics12030532.
[52] N. Klubthawee, P. Adisakwattana, W. Hanpithakpong, S. Somsri, R. Aunpad, A novel, rationally designed, hybrid antimicrobial peptide, inspired by cathelicidin and aurein, exhibits membrane-active mechanisms against Pseudomonas aeruginosa, Sci. Rep. 10 (1) (2020) 9117, https://doi.org/10.1038/s41598-020-65688-5.
[53] C. Zhang, L. Fu, Y. Zhu, Q. Chen, Z. Chen, Y. Chang, Y. Li, M. Yao, X. Huang, L. Jin, X. Gao, Y. Zhang, B. Jin, S. Chou, L. Luo, Antimicrobial activity of novel symmetrical antimicrobial peptides centered on a hydrophilic motif against resistant clinical isolates: in vitro and in vivo analyses, Microbiol. Spectrum 12 (2024) e00265-24, https://doi.org/10.1128/spectrum.00265-24.
[54] H. Hou, J. Wang, J. Wang, W. Tang, A.S. Shaikh, Y. Li, J. Fu, L. Lu, F. Wang, F. Sun, H. Tan, A review of bioactive peptides: chemical modification, structural characterization and therapeutic applications, J. Biomed. Nanotechnol. 16 (12) (2020) 1687–1718, https://doi.org/10.1166/jbn.2020.3001.
[55] P. Zhang, Y. Huang, Y.T. Kwon, S. Li, PEGylated Fmoc-amino acid conjugates as effective nanocarriers for improved drug delivery, Mol. Pharm. 12 (5) (2015) 1680–1690, https://doi.org/10.1021/acs.molpharmaceut.5b00157.

[56] W. Li, N.M. O'Brien-Simpson, M.A. Hossain, J.D. Wade, The 9-fluorenylmethoxy-carbonyl (Fmoc) group in chemical peptide synthesis – its past, present, and future, Aust. J. Chem. 73 (4) (2019) 271–276, https://doi.org/10.1071/CH19427.
[57] A.S. Saghyan, A.F. Mkrtchyan, H.M. Simonyan, N.A. Hovhannisyan, A. M. Hovhannisyan, New generations of optically active non-proteinogenic α-amino acids: synthesis and study, Chem. J. Armenia 69 (1–2) (2016) 1–8.
[58] C. Perez-Iratxeta, M.A. Andrade-Navarro, K2D2: estimation of protein secondary structure from circular dichroism spectra, BMC Struct. Biol. 8 (2008) 25, https://doi.org/10.1186/1472-6807-8-25.
[59] D. Zhao, X. Liu, Purification, identification and evaluation of antioxidant peptides from pea protein hydrolysates, Molecules 28 (7) (2023) 2952, https://doi.org/10.3390/molecules28072952.
[60] N. Saeed, M.R. Khan, M. Shabbir, Antioxidant activity, total phenolic and total flavonoid contents of whole plant extracts Torilis leptophylla L, BMC Complement. Altern. Med. 12 (2012) 221, https://doi.org/10.1186/1472-6882-12-221.
[61] V. Mittova, M. Pirtskhalava, R. Bidzinashvili, M. Vakhania, T. Mindiashvili, M. Kobiashvili, Effects of different drying, extraction methods, and solvent polarity on the antioxidant properties of *Paeonia daurica* subsp. *mlokosewitschii* leaves, MIMM 26 (2) (2023) 66–77, https://doi.org/10.56580/GEOMEDI39.
[62] S. Mitra, A.V. Bhesania Hodiwala, H. Kar, Susceptibility and synergistic effects of guava plant extract and antimicrobial drugs on Escherichia coli, Cureus 16 (1) (2024) e52345, https://doi.org/10.7759/cureus.52345.
[63] A. Galano, G. Mazzone, R. Alvarez-Diduk, T. Marino, J.R. Alvarez-Idaboy, N. Russo, Food antioxidants: chemical insights at the molecular level, Annu. Rev. Food Sci. Technol. 7 (2016) 335–352, https://doi.org/10.1146/annurev-food-041715-033206.
[64] M. Leopoldini, T. Marino, N. Russo, M. Toscano, Antioxidant properties of phenolic compounds: H-atom versus electron transfer mechanism, J. Phys. Chem. A 108 (22) (2004) 4916–4922, https://doi.org/10.1021/jp037247d.
[65] A. Amić, B. Lučić, V. Stepanić, Z. Marković, S. Marković, J.M. Dimitrić Marković, D. Amić, Free radical scavenging potency of quercetin catecholic colonic metabolites: thermodynamics of $2H^+/2e^-$ processes, Food Chem. 218 (2017) 144–151, https://doi.org/10.1016/j.foodchem.2016.09.018.
[66] Y. Xue, Y. Zheng, L. An, Y. Dou, Y. Liu, Density functional theory study of the structure–antioxidant activity of polyphenolic deoxybenzoins, Food Chem. 151 (2014) 198–206, https://doi.org/10.1016/j.foodchem.2013.11.064.
[67] L. Stepanyan, T. Sargsyan, V. Mittova, Z.R. Tsetskhladze, N. Motsonelidze, E. Gorgoshidze, N. Nova, M. Israyelyan, H. Simonyan, F. Bisceglie, L. Sahakyan, K. Ghazaryan, G.N. Roviello, Synthesis, characterization, and biological evaluation of a fluorenyl-methoxycarbonyl-containing thioxo–triazole–bearing dipeptide: antioxidant, antimicrobial, and BSA/DNA binding studies for potential therapeutic applications in ROS scavenging and drug transport, Biomolecules 15 (7) (2025) 933, https://doi.org/10.3390/biom15070933.
[68] L. Verderi, N. Nova, V. Borghesani, M. Tegoni, M. Giannetto, S. Fortunati, L. Ronda, S. Pinelli, P. Mozzoni, M. Nicastro, et al., Cytotoxic ROS-consuming Mn (III) synzymes: structural influence on their mechanism of action, Int. J. Mol. Sci. 26 (1) (2025) 150, https://doi.org/10.3390/ijms26010150.
[69] M.J. Frisch, G.W. Trucks, H.B. Schlegel, G.E. Scuseria, M.A. Robb, J.R. Cheeseman, G. Scalmani, V. Barone, G.A. Petersson, H. Nakatsuji, X. Li, M. Caricato, A. V. Marenich, J. Bloino, B.G. Janesko, R. Gomperts, B. Mennucci, H.P. Hratchian, J. V. Ortiz, A.F. Izmaylov, J.L. Sonnenberg, D. Williams-Young, F. Ding, F. Lipparini, F. Egidi, J. Goings, B. Peng, A. Petrone, T. Henderson, D. Ranasinghe, V. G. Zakrzewski, J. Gao, N. Rega, G. Zheng, W. Liang, M. Hada, M. Ehara, K. Toyota, R. Fukuda, J. Hasegawa, M. Ishida, T. Nakajima, Y. Honda, O. Kitao, H. Nakai, T. Vreven, K. Throssell, J.A. Montgomery Jr., J.E. Peralta, F. Ogliaro, M. J. Bearpark, J.J. Heyd, E.N. Brothers, K.N. Kudin, V.N. Staroverov, T.A. Keith, R. Kobayashi, J. Normand, K. Raghavachari, A.P. Rendell, J.C. Burant, S.S. Iyengar, J. Tomasi, M. Cossi, J.M. Millam, M. Klene, C. Adamo, R. Cammi, J.W. Ochterski, R.L. Martin, K. Morokuma, O. Farkas, J.B. Foresman, D.J. Fox, Gaussian 16, Revision B.01, Gaussian, Inc., Wallingford CT, 2016.
[70] S. Xavier, S. Periandy, K. Carthigayan, S. Sebastian, Molecular docking, TG/DTA, molecular structure, harmonic vibrational frequencies, natural bond orbital and TD-DFT analysis of diphenyl carbonate by DFT approach, J. Mol. Struct. 1125 (2016) 204–216, https://doi.org/10.1016/j.molstruc.2016.06.071.
[71] J. Tomasi, B. Mennucci, R. Cammi, Quantum mechanical continuum solvation models, Chem. Rev. 105 (8) (2005) 2999–3094, https://doi.org/10.1021/cr9904009.
[72] D.S. El-Sayed, S.S. Hassan, L.S. Jassim, et al., Structural and topological analysis of thiosemicarbazone-based metal complexes: computational and experimental study of bacterial biofilm inhibition and antioxidant activity, BMC Chem. 19 (2025) 24, https://doi.org/10.1186/s13065-024-01338-5.
[73] L. Yang, H. Liu, D. Xia, S. Wang, Antioxidant properties of camphene-based thiosemicarbazones: experimental and theoretical evaluation, Molecules 25 (5) (2020) 1192, https://doi.org/10.3390/molecules25051192.
[74] N. González-Mojica, L. Almazán-Sánchez, J.G. García-Torres, I. Santana-Martinez, D. Martínez-Otero, M.A. Sánchez-Carmona, E. Cuevas-Yañez, Oxidation of 1,4-disubstituted-1,2,3-triazoles with H_2O_2-CF_3CO_2H: efficient synthesis of 1,2,3-triazole 3-oxides, Synth. Commun. 49 (5) (2019) 679–687, https://doi.org/10.1080/00397911.2019.1566473.
[75] T.I. Kashar, S.A. Aal, Spectral, DFT–TDDFT computational investigation and biological studies of transition metal complexes of dehydroacetic acid Schiff base, J. Iran. Chem. Soc. 18 (2021) 1625–1640, https://doi.org/10.1007/s13738-020-02134-3.
[76] F. Iemma, U.G. Spizzirri, F. Puoci, R. Muzzalupo, S. Trombino, R. Cassano, S. Leta, N. Picci, pH-Sensitive hydrogels based on bovine serum albumin for oral drug delivery, Int. J. Pharm. 312 (1–2) (2006) 151–157, https://doi.org/10.1016/j.ijpharm.2006.01.010.
[77] Y. Yan, S.Y. Huang, Modeling protein–protein or protein–DNA/RNA complexes using the HDOCK webserver, in: D. Kihara (Ed.), Protein Structure Prediction. Methods in Molecular Biology vol. 2165, Humana, New York, NY, 2020, pp. 301–314, https://doi.org/10.1007/978-1-0716-0708-4_12.
[78] A. Bujacz, Structures of bovine, equine and leporine serum albumin. Biological Crystallography, Acta Crystallogr. D Biol. Crystallogr. 68 (10) (2012) 1278–1289, https://doi.org/10.1107/S0907444912027047.
[79] M.R. Naylor, A.M. Ly, M.J. Handford, D.P. Ramos, C.R. Pye, A. Furukawa, V. G. Klein, R.P. Noland, Q. Edmondson, A.C. Turmon, W.M. Hewitt, J. Schwochert, C.E. Townsend, C.N. Kelly, M.J. Blanco, R.S. Lokey, Lipophilic permeability efficiency reconciles the opposing roles of lipophilicity in membrane permeability and aqueous solubility, J. Med. Chem. 61 (24) (2018) 11169–11182, https://doi.org/10.1021/acs.jmedchem.8b01259.
[80] P. Matsson, B.C. Doak, B. Over, J. Kihlberg, Cell permeability beyond the rule of 5, Adv. Drug Deliv. Rev. 101 (2016) 42–61, https://doi.org/10.1016/j.addr.2016.03.013. PMID:2706.
[81] S. Karoui, O. Khaoua, N. Benbellat, S. Antonczak, A. Messaoudi, Molecular docking, molecular dynamics, pkCSM drug-likeness profiles, toxicity, and DFT study of the antioxidant and anticancer activities of three flavonoid derivatives, ChemistrySelect 9 (40) (2024) e202401776, https://doi.org/10.1002/slct.202401776.
[82] I. Khettache, A. Messaoudi, S. Antonczak, A theoretical study of molecular reactivity in medicinal chemistry: antioxidant properties of isoflavonoid Lupinalbin B in its active forms, J. Indian Chem. Soc. 102 (5) (2025) 101678, https://doi.org/10.1016/j.jics.2025.101678.
[83] O. Khaoua, F. Guenfoud, R. Bendaas, A. Messaoudi, N. Benbellat, In vitro antibacterial, antifungal activities, reactivity, bioactivity, GUSAR, cytotoxicity profiles, molecular docking, and dynamic simulations of quinoline acrylonitrile derivatives, ChemistrySelect 10 (35) (2025) e03272, https://doi.org/10.1002/slct.202503272.
[84] V. Roviello, D. Musumeci, A. Mokhir, G.N. Roviello, Evidence of protein binding by a nucleopeptide based on a thymine-decorated L-diaminopropanoic acid through CD and in silico studies, Curr. Med. Chem. 28 (24) (2021) 5004–5015, https://doi.org/10.2174/0929867328666210201152326.